Aust. J. Phys., 1995, **48**, 469–77

Analysis of the Coulomb-solidification Process in Particle Plasmas*

K. Tachibana and Y. Hayashi

Department of Electronics and Information Science, Kyoto Institute of Technology, Matsugasaki, Sakyo-ku, Kyoto 606, Japan.

Abstract

The Coulomb-solidification process is analysed using Mie-scattering ellipsometry with the assistance of photography and scanning electron microscopy. Spherical monodisperse carbon particles are observed to grow in a methane plasma. The Coulomb-coupling parameter at the liquid-to-solid phase transition is evaluated to be around 200, which is close to the value predicted by a Monte Carlo simulation. The growth of monodisperse particles of μm size having the same charge favours the formation of a Coulomb solid.

1. Introduction

Particles can be suspended in the gas phase for long periods of time when they are negatively charged and trapped in the positive potential of a plasma. Dusty plasmas have been eagerly investigated by many research groups lately (e.g. Selwyn *et al.* 1990; Bouchoule *et al.* 1991; Watanable *et al.* 1992), because particle contamination in processing plasmas can cause severe problems in microelectronics manufacturing. Particle plasmas which contain a substantial number of particles show interesting characteristics which differ from those of ordinary plasma. One noticeable feature is the formation of Coulomb solids, as predicted by theoretical considerations (Ikezi 1986). Triggered by this prediction, three successful results (Hayashi and Tachibana 1994*c*; Chu and I 1994; Thomas *et al.* 1994) were independently published last year, almost at the same time. Coulomb solidification is also of interest to researchers who study space dust, because the existence of Coulomb solids formed from the space dust could be possible, for example, in a planetary ring (Goertz 1989).

An investigation of the phenomenon through either analysis of the phase transition or direct observation of the particles will help to evaluate the forces acting on the particles and how to control them in processing plasmas. The observation of the transition between the Coulomb liquid and the Coulomb solid in a macroscopic (visible) model may also help in understanding the phase transition in solid-state physics. It is also possible to apply the solidified state to tailored particle synthesis, since particles can be produced or coated by plasma chemical vapour deposition (CVD) under controlled conditions.

* Refereed paper based on a presentation to the Third Japan–Australia Workshop on Gaseous Electronics and Its Applications, held at Yeppoon, Queensland, in July 1994.

0004-9506/95/030469$05.00

Recently we succeeded in forming a Coulomb solid from carbon particles injected in a methane plasma and grown to μm size (Hayashi and Tachibana 1994*b*, 1994*c*). In the experiment, particle growth and the density decrease were monitored by means of newly developed Mie-scattering ellipsometry (Hayashi and Tachibana 1994*a*). Discontinuous changes were observed in both the growth rate and the density decrease 25–30 min after particle injection. This period of time matches well with the change from liquid to solid phases verified by photographs taken from an upper viewport.

In this paper, using Mie-scattering ellipsometry and scanning electron microscope (SEM) observations, the Coulomb-solidification process is analysed in more detail by evaluation of the shape, size, distribution, density, and charge of particles. With the data obtained, the change in the Coulomb-coupling parameter can be evaluated in the solidification process.

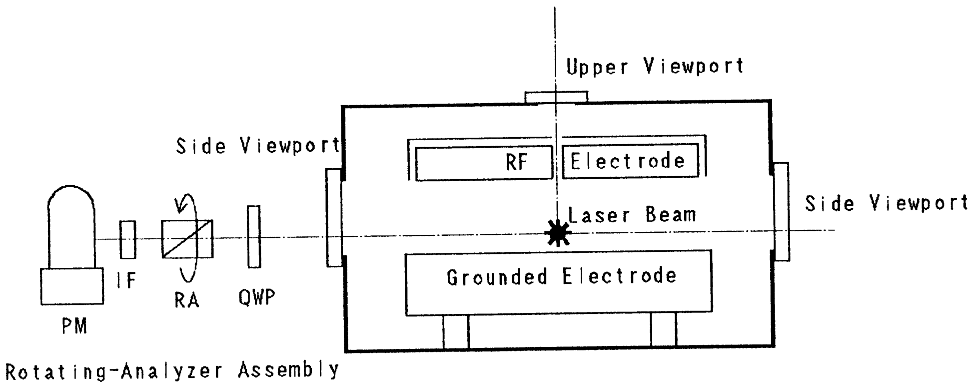

Fig. 1. Schematic of the experimental system (cross-sectional view perpendicular to the laser beam propagation direction): QWP, quarter-wave plate; RA, rotating analyser; IF, interference filter; and PM, photomultiplier.

2. Experimental

As shown in Fig. 1, carbon particles were grown and a Coulomb solid formed in the same plasma CVD reactor as reported earlier (Hayashi and Tachibana 1994*c*). The reactor was equipped with the Mie-scattering elipsometry system (Hayashi and Tachibana 1994*a*). An argon-ion laser operating at 488 nm was used as the light source for Mie-scattering observations. A linearly polarised laser beam at 45° azimuth from the scattering plane propagated through the reactor at a height of 0·6 cm above the grounded electrode, which was placed 2·5 cm below the rf electrode.

Ultra-fine carbon particles were injected into the reactor from one burst of 100 kPa cm^3 methane gas, forming the seeds for growing carbon particles. The gas pressure of the pure methane was 40 Pa and the rf power was 10 W. The gas was introduced into the reactor under a controlled gas flow of 16 standard cm^3 min^{-1} (sccm) in order not to blow away particles trapped in the plasma.

The polarisation state of the Mie-scattered light from particles in the plasma was detected through a rotating-analyser assembly (Hayashi 1990) at 90° from the laser beam. The arrangement of particles was observed at the same time by Mie-scattered light through upper and side viewports.

The shapes of the fully grown carbon particles were observed by SEM. The particles falling after switching off the rf power were collected on a copper fine mesh placed on the grounded electrode.

3. Results

From observations of Mie-scattered light over the whole plasma region, it was seen that ultra-fine carbon particles are suspended around the sheath–plasma boundary near the rf electrode in the early period. As the particles grow by coagulation and coating, they fall by gravity towards the grounded electrode and finally remain around the sheath–plasma boundary near the grounded electrode,

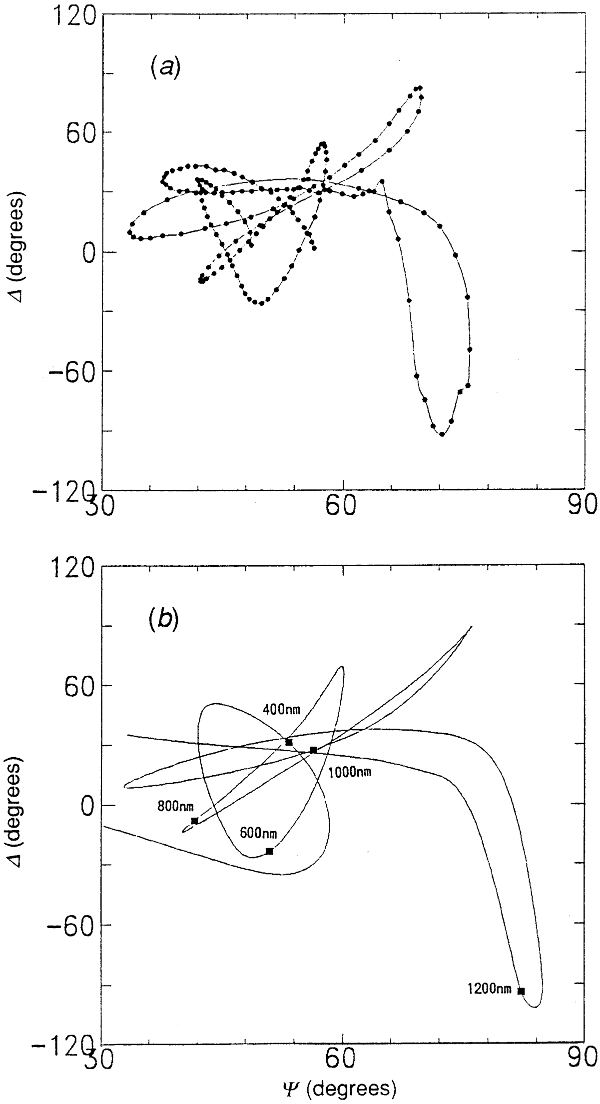

Fig. 2. The (Ψ, Δ) trajectories obtained by (a) experiment and (b) simulation for carbon particle growth. The points in (a) are plotted every 10 s (see text for the parameters used in the simulation).

suspended by a balance of various forces acting on them (e.g. Sommerer *et al.* 1991; Kilgore *et al.* 1993; Perrin *et al.* 1994).

The trajectory of the ellipsometric parameters Ψ and Δ during the growth phase is shown in Fig. 2*a*. The trajectory was simulated theoretically and compared with the experimental result. The simulation was performed by assuming a simple growth model for particles with spherical shape as follows. The size d of the injected seed particles has the log-normal distribution

$$N(d) = \frac{1}{(2\pi)^{\frac{1}{2}}\ln(\sigma)d}\exp\left(-\frac{[\ln(d)-\ln(d_{\mathrm{m}})]^2}{2[\ln(\sigma)]^2}\right), \tag{1}$$

and only the mean diameter of particles d_{m} grow by keeping the geometric standard deviation σ constant (Hayashi and Tachibana 1994*b*). The trajectory calculated with this model fitted experiment better than that calculated by assuming a standard deviation proportional to the mean size. Fig. 2*b* shows the simulated trajectory where the parameters of best fit are 50 nm for the geometric mean size of the initial seed particles injected, 1·5 for the geometric standard deviation and 1·53 for the refractive index of the growing particles. This index is close to that of hydrogenated amorphous carbon (Smith 1984).

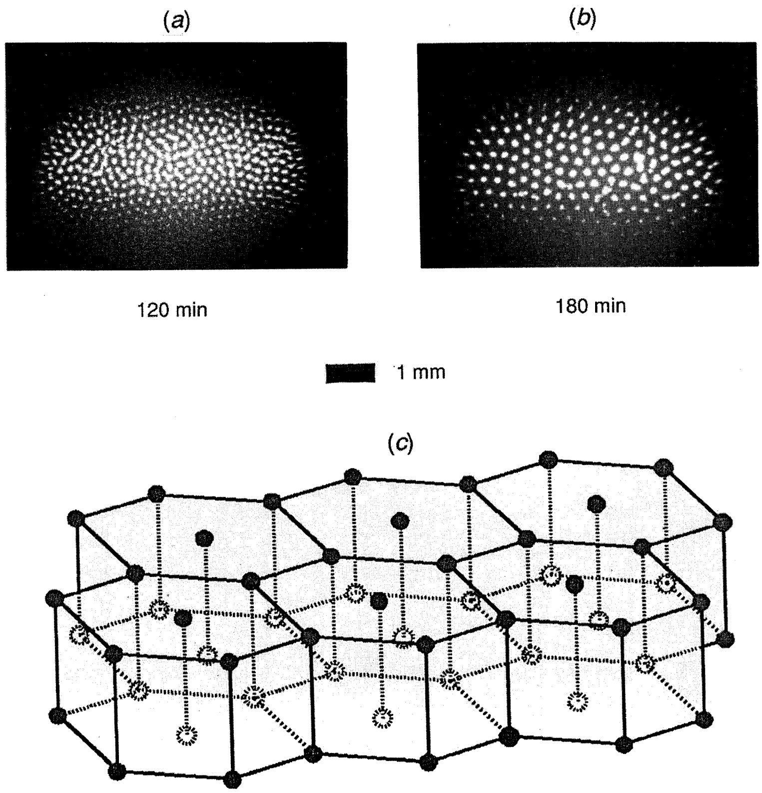

Fig. 3. (*a*) and (*b*) Photographs of the Coulomb solid taken from the upper viewport and (*c*) an image of the three-dimensional structure.

From the photographs taken from the upper or side viewport, the liquid pattern in the laser beam 'freezes' after approximately 30 min. Figs 3*a* and 3*b* show arrangements of particles taken from the upper viewport at 120 and 180 min after the seed particle injection. Inter-particle distances in the plane parallel to the electrodes were determined from the photographs to be 200 μm at 120 min and 290 μm at 180 min. The arrangement of particles was also observed and recorded from the side viewport. From the side and upper viewport photographs, the three-dimensional structure of the particle arrangement was shown to be hexagonal as seen in Fig. 3*c*.

The mean diameter of particles was determined from the correspondence of maximum or minimum Δ values between the experimental trajectory (Fig. 2*a*) and the calculated one (Fig. 2*b*). The particle density was evaluated from the ratio of the experimental Mie-scattering intensity to that in the calculation for each diameter determined, which was calibrated against the density evaluated from the photographs of particle arrangements at 180 min. The effective Wigner–Seitz radius of a particle is defined by $a = (\frac{3}{4}\pi N)^{\frac{1}{3}}$, where N is the particle density. Variations in the mean diameter and radius over time are shown in Fig. 4.

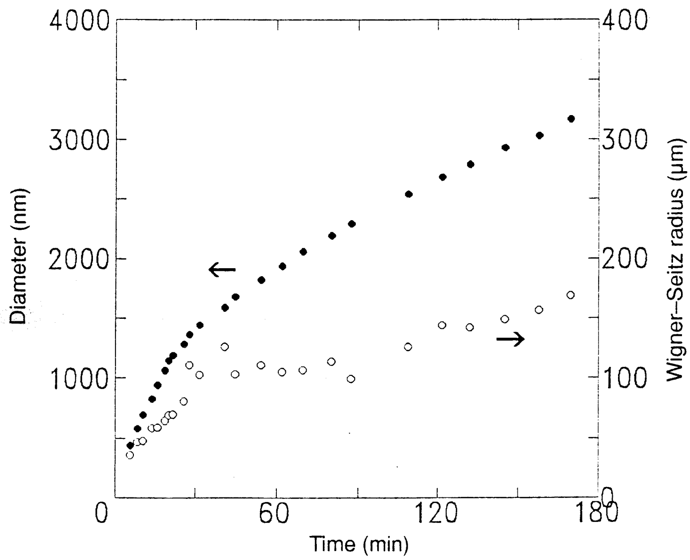

Fig. 4. Time variation of the mean diameter and the Wigner–Seitz radius of particles.

Fig. 5 shows a typical SEM picture of particles trapped in the plasma for 180 min. One of the particles is seen to be spherical with a diameter of $3 \cdot 0$ μm and the other is slightly ellipsoidal with a latitudinal diameter of $3 \cdot 1$ μm and a longitudinal diameter of $3 \cdot 0$ μm. Most other particles observed by SEM were almost spherical with diameters around $3 \cdot 0$ μm. The thickness of the carbon film deposited on a silicon wafer placed on the grounded electrode was measured to be $0 \cdot 16$ μm for the 180 min run.

4. Discussion

From the best-fit simulation of the (Ψ, Δ) trajectory, it appears that all carbon particles grow equally by being coated with hydrogenated amorphous carbon which leads to the formation of the monodisperse particles shown in Fig. 5. The mean diameter of particles at 180 min obtained by the ellipsometric trajectory in Fig. 4 is about $3 \cdot 2\ \mu$m, which matches that in the SEM photograph.

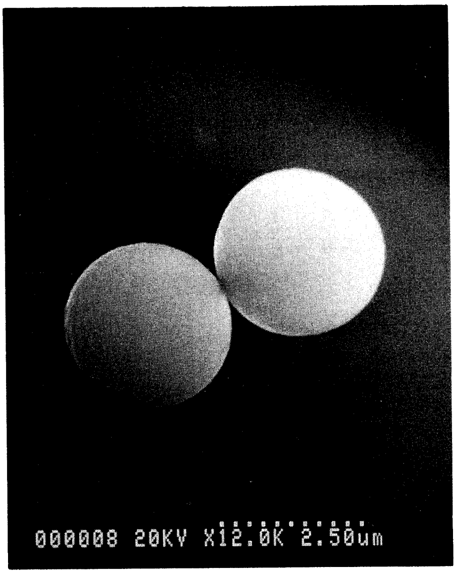

Fig. 5. Typical SEM micrograph of particles trapped in plasma for 180 min.

Discontinuities in the growth rate of the diameter and the Wigner–Seitz radius are seen at 25–30 min in Fig. 4. The change occurs when the arrangement starts to be recognised in the photographic observation. From this correspondence, it is suggested that Coulomb solidification occurs in that period.

The discontinuity in the Wigner–Seitz radius at solidification is considered to occur as follows. Before solidification, the particle density is too high, so that the particles cannot attach enough electrons to couple strongly with each other (Ikezi 1986) and easily escape from the plasma region. However, as the density decreases and the particle charge increases, the particles become bound mutually via positive ions to form the solidified state by reducing the free energy of the state (Slattery *et al.* 1980). Then, their loss is suppressed and the Wigner–Seitz radius becomes almost constant.

The growth rate of particles is constant at $50\ \mathrm{nm\,min}^{-1}$ before solidification, which is much larger than the film deposition rate on the grounded electrode of $0 \cdot 9\ \mathrm{nm\,min}^{-1}$. It slows down to $19\ \mathrm{nm\,min}^{-1}$ just after solidification, and to $5\ \mathrm{nm\,min}^{-1}$ at 180 min. From the discontinuity in particle growth rate, it appears that the growth mechanism changes after solidification. Although details have not yet been clarified for the early fast growth rate, it might be related to coalescence and ion reactions, as has been argued for particle growth in silane plasma (see e.g. Watanable and Shiratani 1993; Perrin 1994). The slower growth after solidification can be attributed to deposition only by neutral radicals. The transport of neutral radicals to particles in the plasma is governed by the free flux due to their thermal motion in contrast to the diffusion to the electrode.

The negative charge $-Q$ $(Q > 0)$ on each particle was evaluated from the particle diameter d and particle density N by the equations

$$1+\frac{1}{2\pi\epsilon_0 d}\,\frac{eQ}{k_{\mathrm{B}}T_{\mathrm{i}}}=\left(\frac{m_{\mathrm{i}}T_{\mathrm{e}}}{m_{\mathrm{e}}T_{\mathrm{i}}}\right)^{\frac{1}{2}}\frac{n_{\mathrm{e}}}{n_{\mathrm{i}}}\exp\left(-\frac{1}{2\pi\epsilon_0\, d}\,\frac{eQ}{k_{\mathrm{B}}T_{\mathrm{e}}}\right), \tag{2a}$$

$$n_{\mathrm{e}}+\frac{Q}{e}N=n_{\mathrm{i}}\,, \tag{2b}$$

where m_{e} is the electron mass, m_{i} the ion mass, T_{e} the electron temperature, T_{i} the ion temperature, n_{e} the electron density and n_{i} the ion density. Equation (1a) is based on the balance between the electron current and the ion current flowing into particles derived from the orbital-motion-limited probe theory (Schott 1970) with $n_{\mathrm{e}} \neq n_{\mathrm{i}}$, under the assumption of a nondrifting Maxwellian velocity distribution for electrons and ions. Equation (1b) comes from the requirement of charge neutrality in plasmas.

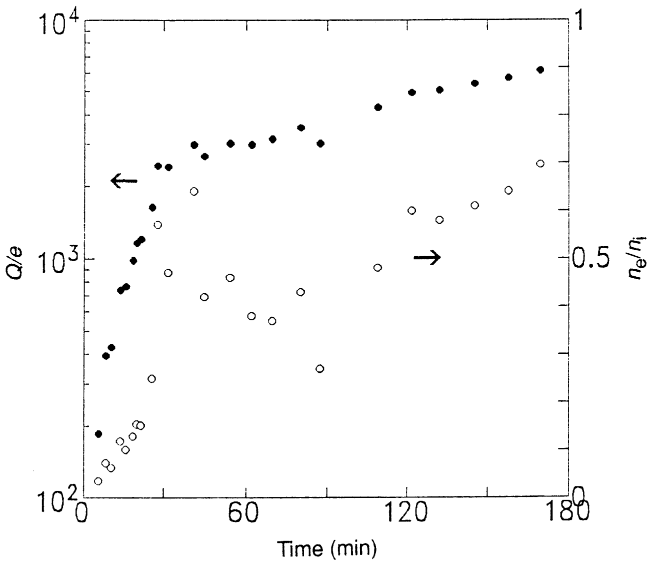

Fig. 6. Estimated time variations of the particle charge Q and the electron density n_{e}, where n_{i} is assumed to be 10^9 cm^{-3}.

Values of Q and n_{e} were calculated from these equations with the assumed values of 10^9 cm^{-3} for the ion density, 3 eV for the electron temperature and 0·03 eV for the ion temperature, which were estimated from values measured previously under similar methane plasma conditions (Tatsuta *et al.* 1991). The results are shown in Fig. 6. It is seen that n_{e} increases before solidification, abruptly increases at the transition, and then becomes almost constant at about 50% of n_{i}. It is also seen that Q increases rapidly before solidification, but then only slowly after the change. These facts suggest the following. Almost all electrons are attached to particles and negative charge in the plasma is carried mainly by particles before solidification because the particle density is too high. With a decrease in particle density, Q and n_{e} increase. An abrupt increase in n_{e} at solidification is caused by an abrupt decrease in particle density, which occurs because the particle distribution in the plasma may be rearranged with the change in the Coulomb interation between particles. After solidification, bound particles rarely escape from the plasma region, so Q and n_{e} change only slowly.

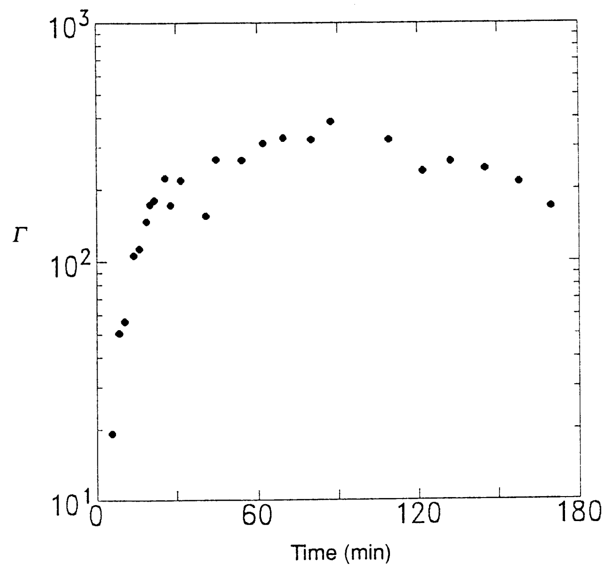

Fig. 7. Estimated time variation of the Coulomb-coupling parameter.

The Coulomb-coupling parameter Γ is defined as the ratio of the Coulomb potential energy of particles to thermal kinetic energy as (Ikezi 1986)

$$\Gamma = \frac{Q^2}{4\pi\epsilon_0\, a}\exp\left(-\frac{a}{\lambda_D}\right)\Big/ k_B\, T\,, \tag{3}$$

where a is the Wigner–Seitz radius defined before, λ_D is the Debye length, calculated to be 40 μm from the ion density and ion temperature given above, and T is the particle temperature. Fig. 7 shows the variation of Γ calculated from the data of Fig. 6 under the assumption $T = T_i$. As shown, Γ increases rapidly at first, reaching about 200 at the time of solidification, and then changes slowly. The Γ value of 200 for the liquid-to-solid phase transition is close to the value of about 170 calculated by a Monte Carlo simulation (Slattery *et al.* 1980). The change in Γ also supports the view that the transition has occurred at 25–30 min.

It has been reported that a Coulomb solid can be formed only with monodisperse particles (McRae and Haymet 1988). From our experiment, it can be concluded that monodisperse spherical particles have been grown by deposition, and this has helped the formation of a Coulomb solid through a liquid phase in the plasma.

5. Conclusion

The process of carbon particle growth and Coulomb solid formation was analysed using Mie-scattering ellipsometry with the assistance of photography of the Coulomb solid and SEM observations of the particles. Carbon particles grow in a methane plasma by uniform coating of hydrogenated amorphous carbon on their surfaces, and consequently they become monodisperse and spherical. A Coulomb solid forms from the carbon particles grown to μm size. The timing of the liquid-to-solid phase transition has been confirmed from changes in the charge Q on each particle, the electron density n_e, and the Coulomb-coupling parameter

Γ, which were derived from the particle diameter d and particle density N. The ratio Γ at the transition is around 200, which is close to the value predicted by a Monte Carlo simulation. The successful formation of a Coulomb solid can be attributed to the growth of monodisperse spherical particles.

References

Bouchoule, A., Plain, A., Boufendi, L., Blondeau, J. Ph., and Laure, C. (1991). *J. Appl. Phys.* **70**, 1991.

Chu, J. H., and I, Lin (1994). *Phys. Rev. Lett.* **72**, 4009.

Goertz, C. K. (1989). *Rev. Geophys.* **27**, 271.

Hayashi, Y. (1990). *Jpn J. Appl. Phys.* **29**, 2514.

Hayashi, Y., and Tachibana, K. (1994*a*). *Jpn J. Appl. Phys.* **33**, L476.

Hayashi, Y., and Tachibana, K. (1994*b*). *Jpn J. Appl. Phys.* **33**, 4208.

Hayashi, Y., and Tachibana, K. (1994*c*). *Jpn J. Appl. Phys.* **33**, L804.

Ikezi, H. (1986). *Phys. Fluids* **29**, 1764.

Kilgore, M. D., Daugherty, J. E., Porteous, R. K., and Graves, D. B. (1993). *J. Appl. Phys.* **73**, 7195.

McRae, R., and Haymet, A. D. J. (1988). *J. Chem. Phys.* **88**, 1114.

Perrin, J. (1994). *Plasma Sources Sci. Technol.* **3**, 252.

Perrin, J., Molinas-Mata, P., and Belenguer, P. (1994). *J. Phys.* D (to be published).

Schott, L. (1970). *In* 'Plasma Diagnostics' (Ed. W. Lochte-Holtgreven), Chap. 11 (Wiley: New York).

Selwyn, G. S., Heidenreich, J., and Haller, K. L. (1990). *Appl. Phys. Lett.* **57**, 1876.

Slattery, W. L., Doolen, G. D., and DeWitt, H. E. (1980). *Phys. Rev.* A **21**, 21.

Smith, F. W. (1984). *J. Appl. Phys.* **55**, 764.

Sommerer, T., Barnes, M. S., Kekker, J. H., McCaughey, M. J., and Kushner, M. J. (1991). *Appl. Phys. Lett.* **59**, 638.

Tatsuta, T., Okuno, T., Tachibana, K., and Tsuji, O. (1991) Eighth Symp. on Plasma Processing, Nagoya, January 1991, p. 77 (Division of Plasma Electronics, Japan Soc. Appl. Phys.: Tokyo).

Thomas, H., Morfill, G. E., Demmel, V., Goree, J., Feuerbacher, B., and Mohlmann, D. (1994). *Phys. Rev. Lett.* **73**, 652.

Watanabe, Y. and Shiratani, M. (1993). *Jpn J. Appl. Phys.* **32**, 3074.

Watanabe, Y., Shiratani, N., and Yamashita, N. (1992). *Appl. Phys. Lett.* **61**, 1510.

Manuscript received 20 October, accepted 18 November 1994